



Astrochemistry of protoplanetary disks: HCN and H₂CO

V. Guzmán¹, K. I. Öberg², J. Huang², R. Loomis³, J. Carpenter⁴, C. Qi²,
R. Le Gal², and J. Pegues²

¹ Instituto de Astrofísica, Ponticia Universidad Católica de Chile, Av. Vicuña Mackenna 4860, 7820436 Macul, Santiago, Chile, e-mail: vguzman@astro.puc.cl

² Harvard-Smithsonian Center for Astrophysics, 60 Garden Street, Cambridge, MA 02138, US

³ National Radio Astronomy Observatory, Charlottesville, VA, United States

⁴ Joint ALMA Observatory (JAO), Alonso de Córdova 3107, Vitacura, Santiago de Chile, Chile

Abstract. Protoplanetary disks are the birthplace of planets. The chemical composition of nascent planets is thus directly linked to the composition and distribution of the material in disks. We present observations of simple organic species detected in protoplanetary disks, including HCN and H₂CO. We used ALMA to observe the two HCN isotopologues, namely H¹³CN and HC¹⁵N, in a sample of six protoplanetary disks with different stellar type and disk structure properties. We measured the ¹⁴N/¹⁵N isotopic ratios and find values between 80 to 160, with no systematic differences between the disks. We also present SMA and ALMA observations of multiple emission lines of H₂CO towards the disk around Herbig Ae star HD163296. We derive the first measurement of the ortho-to-para ratio of H₂CO in a protoplanetary disk, finding a disk-averaged o/p ratio of 1.8 - 2.8, depending on the assumed disk structure. The derived rotational temperature of ~ 24 K is consistent with H₂CO coming from the colder regions in the disk, where the dominant formation pathway is likely grain surface chemistry. We end with a brief discussion about the future directions of disk chemistry studies, inspired by the remarkable structure seen in the dust continuum emission by the DSHARP ALMA Large Program.

Key words. Stars: abundances – Stars: atmospheres – Stars: Population II – Galaxy: globular clusters – Galaxy: abundances – Cosmology: observations

1. Introduction

What sets the composition of nascent planets is a fundamental question in astronomy, and one that is extremely topical considering the large number of exoplanets with very different characteristics that have been discovered in the past years (e.g., Coughlin et al. 2016). We know

that the formation of protoplanetary disks is a natural consequence of star formation. Dust particles in the disk can coagulate to form planetesimals and eventually planets (Testi et al. 2014). The detailed physical and chemical processes involving star and planet formation are, however, not well known. Moreover, our current understanding of the chemical composi-

tion of protoplanetary disks and the evolution of the material from the prestellar gas to the disk phase is very limited.

The molecular inventory in protoplanetary disks is relatively small. Only 36 species, including isotopes, have been detected in disks compared to the ~ 200 species that have been detected in the interstellar medium (McGuire 2018). Most of the new detections have only been possible thanks to the great sensitivity of ALMA. Some examples of the most recent detections are CH_3CN (Öberg et al. 2015), CH_3OH (Walsh et al. 2016), HC^{15}N (Guzmán et al. 2015), HCOOH (Favre et al. 2018), and the rarest CO isotopologue $^{13}\text{C}^{17}\text{O}$ (Booth et al. 2019). Most of these molecular species have weak line emission, and their spatial distribution is thus not well constrained.

Theoretical models predict a chemically stratified disk structure (see right side in Fig. 1) due to the radial and vertical temperature and UV radiation gradients produced by the exposure of disk surfaces to stellar and interstellar radiation, and attenuation of this radiation by dust and gas. In the surface layers the chemistry will be dominated by the stellar and interstellar radiation field. Molecules that are readily photo dissociated by UV radiation (e.g., HCN) will mainly be present in a protected warm molecular layer between the disk surface and the cold midplane. In the cold midplane freeze-out of heavy atoms is expected to be nearly complete, which opens-up chemical pathways to form new species in the gas-phase (e.g. N_2H^+) and on the surface of dust grains (e.g. CH_3OH). Although the bulk of the mass is in form of gas, it is also important to characterize the distribution of dust grains and their interaction with the gas if we want to understand how planets form. Initially, disks are flared and the solid mass consists of micron-size dust particles. During the disk lifetime, dust particles settle in the midplane, migrate and grow to form planetesimals, and eventually planets (see left side in Fig. 1). The DSHARP program recently showed that protoplanetary disks show a very rich disk structure in their millimeter dust emission (Andrews et al. 2018).

Here, we focus on the small organic species HCN and H_2CO . We first present observations

of the HCN isotopologues in a sample of 6 protoplanetary disks (Guzmán et al. 2017). We then show multi-line observations of H_2CO towards the disk around the Herbig Ae star HD 163296 (Guzmán et al. 2018). The observations are presented in section 2 and the main results are summarized in section 3. A discussion and main conclusions are given in section 4.

2. Observations

2.1. HCN isotopologues

The $J = 3 - 2$ lines of H^{13}CN and HC^{15}N were observed with ALMA towards a sample of 6 protoplanetary disks as part of project 2013.1.00226. A detailed description of the observations and data reduction process can be found in Huang et al. (2017) and Guzmán et al. (2017). Briefly, each disk was observed for ~ 20 min on-source. The Band 6 data was first calibrated by the JAO staff using standard proceedings, and then self-calibrated by our team to improve the signal-to-noise ratio. The continuum was then subtracted from the visibilities. The continuum-subtracted visibilities were cleaned with CASA using the CLEAN task, and elliptical masks were used to help the cleaning process. The data were regridded to a spectral resolution of 0.5 km s^{-1} , and the typical beam of the cleaned images is $\sim 0.5''$.

The sample includes disks with luminosities that span an order of magnitude (see Table 1). Four disks are host by T Tauri stars and two of them by Herbig Ae stars. In addition, the sample includes transitional disks with inner holes resolved at millimeter wavelength (LkCa 15 and V4046 Sgr), and full disks (AS 209, IM Lup, MWC 480 and HD163296). These disks thus have very different physical properties, in particular the gas temperature. The purpose of such a sample is to determine the disk averaged $^{14}\text{N}/^{15}\text{N}$ ratio in HCN in a diverse sample of disks.

2.2. H_2CO in HD163296

A total of five H_2CO lines were observed with SMA, three of them ortho lines and two of

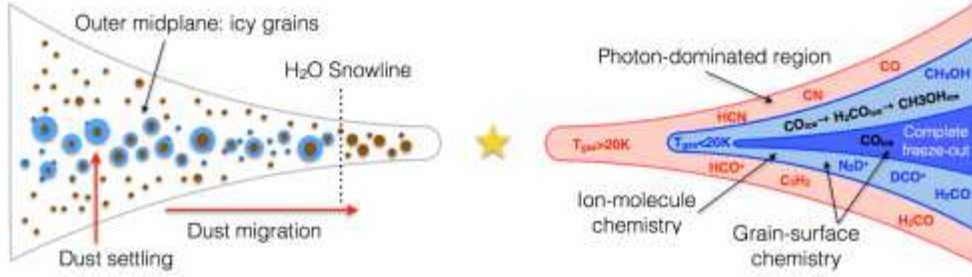


Fig. 1. Distribution and chemistry of the dust (left) and gas (right) in protoplanetary disks. Disk are originally flared, and dust grains eventually settle in the midplane, grow through coagulation and migrate radially towards the star. Density and temperature vary both radially and vertically, producing a chemical stratification of the disk. The chemistry in the surface layers is dominated by UV-photons. Towards the cold outer midplane, molecules freeze-out onto dust grains opening new formation pathways on grain surfaces. The inner midplane (interior to the snowline) is too warm for ices to form.

Table 1. Star and disk properties in the sample.

| Source | Distance pc | Spectral type | Age Myr | M _★ M _☉ | L _★ L _☉ | Disk Incl. deg | Disk PA deg | M _{disk} M _☉ |
|------------------|----------------|------------------|------------|----------------------------------|----------------------------------|-------------------|----------------|-------------------------------------|
| <i>T Tauri</i> | | | | | | | | |
| AS 209 | 126 | K5 | 1.6 | 0.9 | 1.5 | 38 | 86 | 0.015 |
| IM Lup | 161 | M0 | 1 | 1.0 | 0.93 | 50 | 144.5 | 0.17 |
| LkCa 15 | 140 | K3 | 3-5 | 0.97 | 0.74 | 52 | 60 | 0.05-0.1 |
| V4046 Sgr | 72 | K5,K7 | 24 | 1.75 | 0.49,0.33 | 33.5 | 76 | 0.028 |
| <i>Herbig Ae</i> | | | | | | | | |
| MWC 480 | 142 | A4 | 7 | 1.65 | 11.5 | 37 | 148 | 0.11 |
| HD 163296 | 122 | A1 | 4 | 2.25 | 30 | 48.5 | 132 | 0.17 |

Note: Table reproduced from Huang et al. (2017), where a complete list of references is given.

them para lines. A description of the observations for the lines at 281 and 225 GHz can be found in Qi et al. (2013). The 218, 290, and 300 GHz were observed in March 2014 in the sub-compact array configuration. The data were first calibrated with the MIR software package, using standard procedures. The data were then cleaned in CASA, using circular masks to help the cleaning process, and a robust parameter of 2 to improve the sensitivity. The data were regridded to a spectral resolution of 0.6 km s⁻¹. The beam of the cleaned images varies from 3'' to 8''. For this study, we complemented the SMA observations with higher-angular resolution ALMA observations of the H₂CO line at 290 GHz. A description

of these observations (project 2012.1.00681) can be found in Qi et al. (2015). The data was first calibrated by JAO staff, and further self-calibrated by our team. The continuum subtracted visibilities were cleaned in CASA, using a Keplerian mask. The beam of the final ALMA image is ~ 1''.

3. Results

3.1. A survey of H¹³CN and HC¹⁵N in protoplanetary disks

Figure 2 shows the observations of the dust continuum emission (upper panels) and HCN isotopologue emission (bottom panels) for the

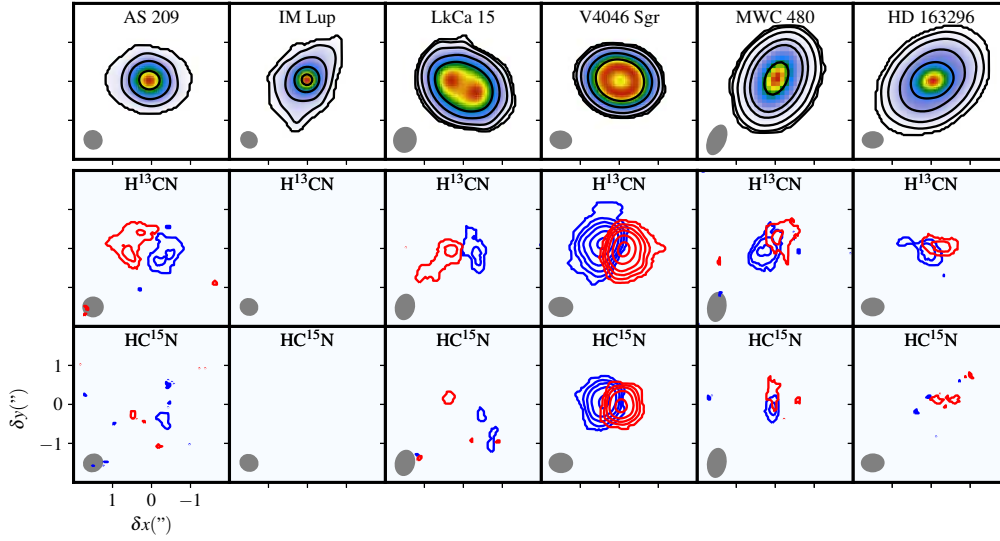


Fig. 2. Dust continuum emission (upper panels). Contour levels correspond to 3, 10, 30, 100, 200, 400 and $800\times\text{rms}$. Middle: Moment zero maps for H^{13}CN and HC^{15}N , integrated over the red- and blue-shifted parts of the line (middle panels). Noise below 2 mJy beam^{-1} has been clipped to produce the moment zero maps. Contour levels correspond to 3, 5, 7, 10, 15, 20 and 30σ . For HC^{15}N contour levels start at 2σ .

full disk sample. Although for some of the disks the emission is almost washed out in the integrated intensity maps, from careful inspection of the channel maps we find that H^{13}CN is detected towards 5 of the 6 disks. H^{13}CN is not detected towards IM Lup. The weaker HC^{15}N isotopologue is detected towards V4046 Sgr, MWC 480 and HD 163296, and only tentatively detected towards AS 209, and not detected towards IM Lup.

We extracted disk integrated fluxes using elliptical masks centered on the disk center and considering their orientation that is given by the inclination and position angle of the disks (see Table 1). These fluxes were then used to compute the $\text{H}^{13}\text{CN}/\text{HC}^{15}\text{N}$ abundance ratio assuming LTE. We obtain $\text{H}^{13}\text{CN}/\text{HC}^{15}\text{N}$ abundance ratios that span from 1.2 to 2.2 with an average of 1.8 across the disk sample. A standard $^{12}\text{C}/^{13}\text{C}$ isotopic ratio of 70 was then assumed to derive the $^{14}\text{N}/^{15}\text{N}$ ratio. We find that all the disks present cometary-like $^{14}\text{N}/^{15}\text{N}$ values, spanning from 83 to 156 with an average of 124 (see Fig. 3). We find no correlation

between the inferred disk averaged N fractionation ratios with the stellar or disk parameters.

All the disks present very similar disk-averaged N fractionation ratios. However, one could expect to find radial or vertical variations within each disk. To investigate this we modeled the radial dependence of the HCN isotopologue emission in the brightest disk in our sample: V4046 Sgr. We first build the disk structure based on the model of Rosenfeld et al. (2013) and used a simple power-law function to model the abundances of H^{13}CN and HC^{15}N in the disk (see Guzmán et al. 2017). We used the RADMC-3D code (Dullemond 2012) to perform the radiative transfer and then created simulated visibilities using the `vis_sample` package¹. The best-fit parameters (the abundance at 100 au and the power-law index of the emission) were found in the $u-v$ plane, using the `emcee` package (Foreman-Mackey et al. 2013) to sample the parameter space.

The best-fit $\text{H}^{13}\text{CN}/\text{HC}^{15}\text{N}$ abundance ratio goes from 1.1 ± 0.1 to 2.0 ± 0.3 at 10

¹ https://pypi.python.org/pypi/vis_sample

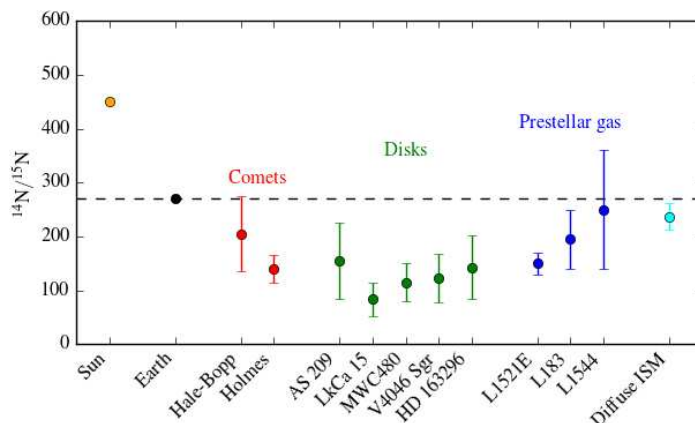


Fig. 3. The observed $^{14}\text{N}/^{15}\text{N}$ isotopic ratios in disks are similar to what is observed in comets and in the cold ISM, which is consistent with the inheritance scenario for the origin of organics in the solar system (Guzmán et al. 2017).

and 40 au, respectively. Assuming a $^{12}\text{C}/^{13}\text{C}$ isotopic ratio of 70, this corresponds to a $^{14}\text{N}/^{15}\text{N}$ fractionation ratio of 76 ± 25 and 142 ± 47 , respectively. The observations towards V4046 Sgr thus suggests an increasing $\text{H}^{13}\text{CN}/\text{HC}^{15}\text{N}$ ratio with radius, which is consistent with higher N fractionation in the inner disk due to selective photo-dissociation. According to chemical models, this process dominates the N fractionation in disks (Visser et al. 2018).

3.2. Multi-line observations of H_2CO in the HD163296 disk

The SMA observations of the 5 H_2CO lines are shown in Fig. 5. The upper panels show the velocity integrated maps, while the bottom panels show the red- and blue-shifted part of the emission to display the Keplerian rotation of the disk. The H_2CO emission shows a ring-like spatial distribution. This can be seen by the off-centered emission in the SMA maps, and corroborated by the higher angular resolution ALMA observations (see Guzmán et al. 2018). Indeed, the deprojected radial profile of the H_2CO line observed with ALMA shows a central depression, a peak of emission near ~ 100 au, and a bump-like structure at ~ 400 au. A similar H_2CO radial profile

has been observed towards other disks (e.g., Loomis et al. 2015; Öberg et al. 2017).

To investigate the excitation of the H_2CO emission, we extracted disk-integrated fluxes using a circular mask with a $6''$ radius, and build a rotational diagram with the three ortho lines (see Fig. 4). We find a rotational temperature of ~ 25 K, which is consistent with the

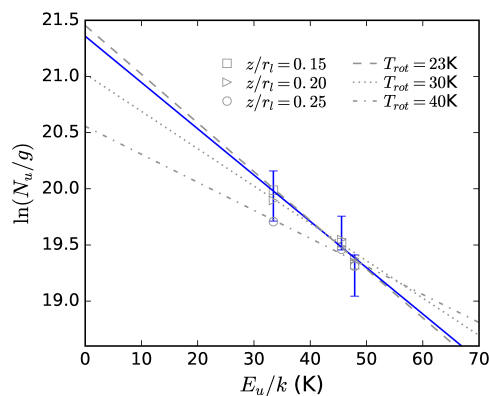


Fig. 4. Rotational diagram of the ortho- H_2CO lines observed towards the HD 163296 disk with the SMA. The blue error bars and the solid line correspond to the observations. The gray markers and lines show the best-fit models. Three models are considered, for different lower boundaries. Figure adapted from (Guzmán et al. 2018).

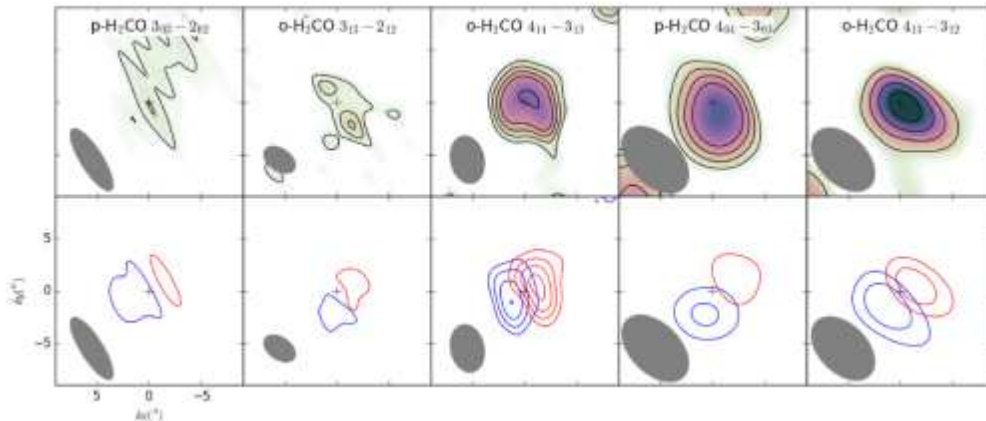


Fig. 5. SMA observations of H_2CO towards the disk around Herbig Ae star HD163296. Velocity integrated line emission (top panels), red- and blue-shifted parts of the emission (middle panels). Contour levels correspond to 3,7,10,20 \times rms. Figure adapted from (Guzmán et al. 2018).

results of Carney et al. (2017). These results suggest that the bulk H_2CO emission arises in the cold layers of the disk.

To derive a disk-averaged H_2CO o/p ratio, we modeled the H_2CO line emission for the HD 163296 disk in a similar way that was done for the HCN isotopologues in the previous section. For this, we use the disk structure presented in Qi et al. (2011). We first use the ALMA observations to find the best-fit parameters of the H_2CO abundance structure in the disk. We then use the five SMA lines to find disk-averaged H_2CO o/p ratio, keeping the spatial distribution of H_2CO constant. We ran 3 sets of models, changing the lower boundary of the emission (z/r_l). The inferred o/p values are 1.8 – 2.8 within 1σ , depending on the assumed lower boundary. The best-fit is obtained when H_2CO is located closer to the midplane (i.e., $z/r_l = 0.15$), which gives a disk-averaged o/p of 2.5.

4. Discussion and conclusions

4.1. The origin of N fractionation ratios in disks

We have shown that the weak HCN isotopologue lines are detected in several disks. Despite the very different physical conditions

of the disks, they all display similar N fractionation levels (the inferred disk-averaged $^{14}\text{N}/^{15}\text{N}$ ratios within the disk sample varies from 50 to 130 within $\sim 1\sigma$). No significant difference is observed between full and transitional disks, or between the youngest (few Myrs) and oldest (~ 10 Myr) disks. This suggests that the N isotopic ratio is either inherited from the prestellar gas, or that this ratio is set very early in the protoplanetary disk life. The observed N fractionation ratios are also very similar to what is observed in the cold gas and in comets (see Fig. 3). For example, observations of 18 comets from the Oort cloud and the Kuiper Belt show low and consistent $^{14}\text{N}/^{15}\text{N}$ ratios in HCN of 100 – 250 (Mumma & Charnley 2011).

Resolved observations of N isotopologues can help to elucidate between different origins for the material in protoplanetary disks. In particular for HCN, we can expect a flat fractionation ratio across the disk if most of HCN is inherited from the prestellar gas and the chemistry is not altered significantly during the disk phase. If, on the other hand, the fractionation profile increases or decreases with radius it will suggest that disk chemistry is active and does modify the N fractionation profile during the disk phase. There are two main pathways to enrich the gas in HC^{15}N in disks. The first one

is through isotope exchange reactions in the cold gas, and the second is through selective photo-dissociation of the main HCN isotopologue compared to the less abundant HC¹⁵N isotopologue. The former will be more important in the colder outer part of the disk, while the latter will be more important in regions directly exposed to UV radiation, i.e., in the inner regions of the disk. We can therefore expect a decreasing N fractionation profile if the cold pathway dominates the formation of HC¹⁵N in the disk, and an increasing N fractionation profile with radius if selective photo-dissociation dominates. The observations towards V4046 Sgr show a tentatively increasing ¹⁴N/¹⁵N ratio with radius. The term tentative is used here because the observations have a resolution of $\sim 0.5''$, and does not fully resolve the fractionation profile in the disk. These results suggest that in situ disk chemistry is active in disks, and will contribute to the observed fractionation patterns. However, higher angular resolution observations are needed to corroborate this trend. Moreover, observations towards other disks are needed to see if this is a unique characteristic of the V4046 Sgr disk or selective photo-dissociation is indeed the dominant fractionation pathway in most protoplanetary disks.

4.2. The first measurement of the H₂CO o/p in disks

H₂CO is a relatively complex species (a precursor to methanol) and can form both in the gas-phase, through reactions of CH₃ with H₂, and on the surface of dust grains, through the successive hydrogenation of CO (e.g. Guzmán et al. 2011). The dominant formation pathway in disks, however, is not clear. Understanding this is important because H₂CO is bright and readily detected in protoplanetary disks (Pegues et al., submitted), while most complex species are harder to detect due to their intrinsic weaker line emission (e.g., Walsh et al. 2016). H₂CO observations can therefore open a window onto the cold organic reservoir in the midplane of disks, which is the place where planets form. However, as mentioned above, we first need to fully understand its dominant

formation pathway and where the emission is coming from: the cold layers just above the midplane or the warmer layers in the surface of the disk. One way to answer this question is to measure the o/p ratio of H₂CO, as it is believed that it can provide information on the formation conditions of the molecule. Carrying-out such measurements is not easy as multiple lines are needed to be able to disentangle between the high-temperature value of 3 and lower values. Here, we have presented a first attempt to measure the disk-integrated H₂CO o/p value in one disk with bright H₂CO emission. Considering different H₂CO spatial distributions, we derive a range of values going from 1.7 to 2.8, which correspond to spin temperatures of 11–22 K. This temperature is consistent with the measured excitation temperature of ~ 24 K. These results suggest that the observed emission arises in the colder layers of the disk, and that the bulk of H₂CO forms on grain surfaces by CO hydrogenation. This is also what current chemical models of disks predict (e.g., Loomis et al. 2015).

The true meaning of o/p ratios is, however, not clear. In particular, it is not clear whether low o/p ratios are indeed indicative of ice formation. Laboratory experiments have shown that H₂ has the high-temperature o/p value of 3 after it forms on water ices at < 10 K, but the o/p ratio would decrease if H₂ was re-trapped in the ice (Watanabe et al. 2010). The conversion of water o/p ratios was also investigated in the laboratory by Hama et al. (2016), who found a value of 3 when H₂O ice is thermally desorbed, no matter if the molecule is formed in situ at 10 K or simply deposited onto the ice, and when H₂O is photodesorbed. Future observations of H₂CO lines at higher-angular resolution will allow us to measure the o/p ratio profile in the disk. A direct comparison of the o/p ratio with the gas temperature structure of the disk at different radii will help us to elucidate what information is actually encoded in o/p measurements.

4.3. Future directions

The field of chemistry in disks has grown largely since the development of ALMA.

However, much remains to be explored. Here I list two directions we should try to follow in the next years:

- So far, we have focused on detailed studies of only a handful of sources, normally the brightest and nearest ones for obvious reasons. Extending these studies to larger samples is needed to ensure our results are not biased and to be able to derive more general conclusions about the composition and distribution of key molecular species in disks.
- The results from the DSHARP Program (Andrews et al. 2018) have shown that rings, gaps and spirals are common features in disks. A natural question is what the structure of the gas component in disks will look like when observed with higher angular resolution. Some of the questions we want to address are: what is the distribution of key organic species in disks? how sensitive is the chemistry to the distribution of the dust? which species are most sensitive? Finally, planet formation of earth-like planets takes place in the inner part of the disk, while most of our current observations (with beams $< 0.5''$) are most sensitive to the outer part of the disk. Higher angular resolution observations will tell us how the chemistry in the *inner* part of the disk looks like.

Acknowledgements. V.V.G. acknowledges support from FONDECYT Iniciación through grant 11180904. V.V.G. and J.C acknowledge support from the National Aeronautics and Space Administration under grant No. 15XRP15 20140 issued through the Exoplanets Research Program.

References

- Andrews, S. M., Huang, J., Pérez, L. M., et al. 2018, *ApJ*, 869, L41
- Booth, A. S., Walsh, C., Ilee, J. D., et al. 2019, arXiv e-prints, arXiv:1908.0504
- Carney, M. T., Hogerheijde, M. R., Loomis, R. A., et al. 2017, arXiv:1705.10188
- Coughlin, J. L., Mullally, F., Thompson, S. E., et al. 2016, *ApJS*, 224, 12
- Dullemond, C. P. 2012, *Astrophysics Source Code Library*, ascl:1202.015
- Favre, C., Fedele, D., Semenov, D., et al. 2018, *ApJ*, 862, L2
- Foreman-Mackey, D., et al. 2013, *PASP*, 125, 30
- Guzmán, V., Pety, J., Goicoechea, J. R., et al. 2011, *A&A*, 534, A49
- Guzmán, V. V., Öberg, K. I., Loomis, R., et al. 2015, *ApJ*, 814, 53
- Guzmán, V. V., Öberg, K. I., Huang, J., et al. 2017, *ApJ*, 836, 30
- Guzmán, V. V., Öberg, K. I., Carpenter, J., et al. 2018, *ApJ*, 864, 170
- Hama, T., Kouchi, A., & Watanabe, N. 2016, *Science*, 351, 65
- Huang, J., Öberg, K. I., Qi, C., et al. 2017, *ApJ*, 835, 231
- Loomis, R. A., Cleeves, L. I., Öberg, K. I., et al. 2015, *ApJ*, 809, L25
- McGuire, B. A. 2018, *ApJS*, 239, 17
- Mumma, M. J., & Charnley, S. B. 2011, *ARA&A*, 49, 471
- Öberg, K. I., Guzmán, V. V., Furuya, K., et al. 2015, *Nature*, 520, 198
- Öberg, K. I., Guzmán, V. V., Merchantz, C. J., et al. 2017, *ApJ*, 839, 43
- Rosenfeld, K. A., et al. 2013, *ApJ*, 775, 136
- Qi, C., D'Alessio, P., Öberg, K. I., et al. 2011, *ApJ*, 740, 84
- Qi, C., Öberg, K. I., & Wilner, D. J. 2013, *ApJ*, 765, 34
- Qi, C., Öberg, K. I., Andrews, S. M., et al. 2015, *ApJ*, 813, 128
- Testi, L., Birnstiel, T., Ricci, L., et al. 2014, in *Protostars and Planets VI*, eds. H. Beuther et al. (Univ. Arizona Press, Tucson), 339
- Visser, R., Bruderer, S., Cazzoletti, P., et al. 2018, *A&A*, 615, A75
- Walsh, C., Loomis, R. A., Öberg, K. I., et al. 2016, *ApJ*, 823, L10
- Watanabe, N., Kimura, Y., Kouchi, A., et al. 2010, *ApJ*, 714, L233